This work was written as part of one of the author's official duties as an Employee of the United States Government and is therefore a work of the United States Government. In accordance with 17 U.S.C. 105, no copyright protection is available for such works under U.S. Law. Access to this work was provided by the University of Maryland, Baltimore County (UMBC) ScholarWorks@UMBC digital repository on the Maryland Shared Open Access (MD-SOAR) platform.

Please provide feedback

Please support the ScholarWorks@UMBC repository by emailing scholarworks-group@umbc.edu and telling us what having access to this work means to you and why it's important to you. Thank you.

Ultraviolet surface-enhanced Raman scattering at the plasmonic band edge of a metallic grating

Nadia Mattiucci,[1] Giuseppe D'Aguanno,[1,*] Henry O. Everitt,[2] John V. Foreman,[2] John M. Callahan,[1] Milan C. Buncick,[1] and Mark J. Bloemer[2]

[1]*AEgis Tech., Nanogenesis Division 410 Jan Davis Dr, Huntsville, Alabama 35806, USA*
[2]*Charles M. Bowden Laboratory, Army Aviation and Missile Research, Development, and Engineering Center, Redstone Arsenal, Alabama 35898, USA*
[*]*giuseppe.daguanno@us.army.mil*

Abstract: Surface-enhanced Raman Scattering (SERS) is studied in sub-wavelength metallic gratings on a substrate using a rigorous electromagnetic approach. In the ultraviolet SERS is limited by the metallic dampening, yet enhancements as large as 10^5 are predicted. It is shown that these enhancements are directly linked to the spectral position of the plasmonic band edge of the metal/substrate surface plasmon. A simple methodology is presented for selecting the grating pitch to produce optimal enhancement for a given laser frequency.

©2012 Optical Society of America

OCIS codes: (240.6695) Surface-enhanced Raman scattering; (240.6680) Surface plasmons; (310.6628) Subwavelength structures, nanostructures; (260.7190) Ultraviolet.

References and links

1. M. Fleischmann, P. J. Hendra, and A. J. McQuillan, "Raman spectra of pyridine adsorbed at a silver electrode," Chem. Phys. Lett. **26**(2), 163–166 (1974).
2. D. L. Jeanmaire and R. P. Van Duyne, "Surface Raman spectroelectrochemistry. Part I. heterocyclic, aromatic and aliphatic amines adsorbed on the anodized silver electrode," J. Electroanal. Chem. **84**(1), 1–20 (1977).
3. M. G. Albrecht and J. A. Creighton, "Anomalously intense Raman spectra of pyridine at a silver electrode," J. Am. Chem. Soc. **99**(15), 5215–5217 (1977).
4. K. Kneipp, M. Moskovits, and H. Kneipp, eds., *Surface enhanced Raman scattering* (Springer, 2006).
5. K. Kneipp, Y. Wang, H. Kneipp, L. Perelman, I. Itzkan, R. Dasari, and M. Feld, "Single molecule detection using surface-enhanced Raman scattering (SERS)," Phys. Rev. Lett. **78**(9), 1667–1670 (1997).
6. A. Otto, I. Mrozek, H. Grabhorn, and W. Akemann, "Surface-enhanced Raman scattering," J. Phys.: Condens. Mat. **4**(5), 1143–1212 (1992).
7. M. Kahl and E. Voges, "Analysis of plasmon resonance and surface-enhanced Raman scattering on periodic silver structures," Phys. Rev. B **61**(20), 14078–14088 (2000).
8. M. I. Stockman, V. M. Shalaev, M. Moskovits, R. Botet, and T. F. George, "Enhanced Raman scattering by fractal clusters: Scale-invariant theory," Phys. Rev. B Condens. Matter **46**(5), 2821–2830 (1992).
9. F. J. García-Vidal and J. B. Pendry, "Collective theory for surface enhanced Raman scattering," Phys. Rev. Lett. **77**(6), 1163–1166 (1996).
10. D. L. Mills, *Nonlinear optics* (Springer-Verlag, 1998).
11. E. V. Efremov, F. Ariese, and C. Gooijer, "Achievements in resonance Raman spectroscopy review of a technique with a distinct analytical chemistry potential," Anal. Chim. Acta **606**(2), 119–134 (2008).
12. S. A. Asher, "UV resonance Raman studies of molecular structure and dynamics: applications in physical and biophysical chemistry," Annu. Rev. Phys. Chem. **39**(1), 537–588 (1988).
13. A. Taguchi, N. Hayazawa, K. Furusawa, H. Ishitobi, and S. Kawata, "Deep-UV tip-enhanced Raman scattering," J. Raman Spectrosc. **40**(9), 1324–1330 (2009).
14. T. Dörfer, M. Schmitt, and J. Popp, "Deep UV surface enhanced Raman scattering," J. Raman Spectrosc. **38**(11), 1379–1382 (2007).
15. X. Zhou, Y. Fang, and P. Zhang, "A new substrate for surface enhanced Raman scattering of dye Sudan molecules," Spectrochim. Acta A Mol. Biomol. Spectrosc. **67**(1), 122–124 (2007).
16. Z.-L. Yang, Q.-H. Li, B. Ren, and Z.-Q. Tian, "Tunable SERS from aluminium nanohole arrays in the ultraviolet region," Chem. Commun. (Camb.) **47**(13), 3909–3911 (2011).
17. E. D. Palik, *Handbook of optical constants of solids* (Academic Press Inc., 1991).
18. H. Raether, *Surface plasmons* (Springer Tracts in Modern Physics- Berlin, 1988).
19. L. Li, "Use of Fourier series in the analysis of discontinuous periodic structures," J. Opt. Soc. Am. A **13**(9), 1870 (1996).
20. G. D. Aguanno, N. Mattiucci, M. J. Bloemer, D. deCeglia, M. A. Vincenti, and A. Alù, "Transmission resonances in plasmonic metallic gratings," J. Opt. Soc. Am. B **28**, 253 (2011).
21. L. D. Landau and E. M. Lifshitz, *Electrodynamics of continuous media* (Pergamon, 1960).

#158512 - $15.00 USD Received 21 Nov 2011; revised 30 Dec 2011; accepted 30 Dec 2011; published 12 Jan 2012
(C) 2012 OSA

22. W. L. Barnes, T. W. Preist, S. C. Kitson, and J. R. Sambles, "Physical origin of photonic energy gaps in the propagation of surface plasmons on gratings," Phys. Rev. B Condens. Matter **54**(9), 6227–6244 (1996).
23. C. Kittel, *Quantum theory of solids* (Wiley, 1963).
24. Note that the Raman enhancement calculated as the fourth power of the absolute value of the electric field of the pump is just a first order approximation. A more accurate calculation should take into account of the enhancement at the pump frequency ω_L and the enhancement at the emitted frequency ω_S as Raman-enhancement=$\left\langle \left|E(\vec{r},\omega_L)/E_0\right|^2 \left|E(\vec{r},\omega_S)/E_0\right|^2 \right\rangle_{slit}$. See for example Ref. 4. For more details the reader can consult Ref. 6 and also: S. Franzen, "Intrinsic limitations of the $|E|^4$ dependence of the enhancement factor for surface-enhanced Raman scattering," J. Phys. Chem. C **113**, 5912 (2009).
25. A. Yariv and P. Yeh, *Optical waves in crystals* (John Wiley, 1984).
26. R. K. Hart, "The Oxidation of Aluminium in Dry and Humid Oxygen Atmospheres," Proc. R. Soc. London, Ser. A **236**, 68 (1956).
27. H. P. Godard, "Oxide Film Growth over Five Years on Some Aluminum Sheet Alloys in Air of Varying Humidity at Room Temperature," J. Electrochem. Soc. **114**(4), 354 (1967).
28. J. A. Dieringer, A. D. McFarland, N. C. Shah, D. A. Stuart, A. V. Whitney, C. R. Yonzon, M. A. Young, X. Zhang, and R. P. Van Duyne, "Surface enhanced Raman spectroscopy: new materials, concepts, characterization tools, and applications," Faraday Discuss. **132**, 9–26 (2006).
29. P. C. Wu, C. G. Khoury, T.-H. Kim, Y. Yang, M. Losurdo, G. V. Bianco, T. Vo-Dinh, A. S. Brown, and H. O. Everitt, "Demonstration of surface-enhanced Raman scattering by tunable, plasmonic gallium nanoparticles," J. Am. Chem. Soc. **131**(34), 12032–12033 (2009).

1. Introduction

Since its first observation [1] and discovery [2,3], surface-enhanced Raman scattering (SERS) has been widely studied both theoretically and experimentally [4] due to a large variety of potential applications in chemical and biological sensing [5]. SERS is commonly attributed to two mechanisms: a) enhancement in polarizability and b) electromagnetic enhancement. The former are due to chemical effects such as charge-transfer excited states [6], while the latter are due to the excitation of surface plasmons (SPs) on a periodically patterned metal surface [7] or localized plasmons over a rough metal surface [8,9].

Because Raman scattering cross sections approximately scale as the fourth power of the laser frequency [10] ultraviolet SERS spectroscopy should produce much stronger signals than traditional visible or infrared wavelength SERS. These signals may be further enhanced in certain proteins and nucleic acids that exhibit an electronic resonance in the ultraviolet (UV) region [11, 12]. Furthermore, an analyte's UV SERS spectra generally will not overlap with its fluorescence spectra, thereby enabling better recognition specificity through the simultaneous measurement of both [13]. UV SERS has been experimentally studied for roughened aluminum (Al) surfaces in Refs [14,15]. and numerically studied for an array of nano-holes in Ref [16].

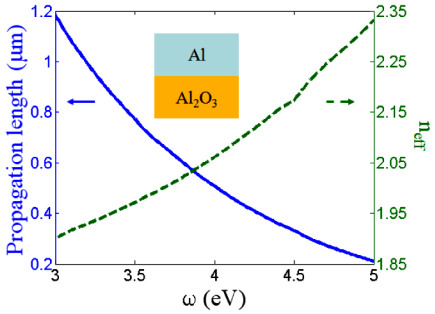

Fig. 1. Propagation length (left y-axis) and effective index (right y-axis) vs. frequency in the UV for a SP at an Al/Al_2O_3 interface.

However, the study of SERS in the UV poses several challenges. First, the most commonly used metals for SERS, silver and gold, do not have a negative real part of the electric permittivity in the frequency range of interest. Second, even for metals like aluminum (Al) which does posses a negative electric permittivity in the UV, the SP will be severely dampened in that frequency range due to the large value of the imaginary part of the electric

#158512 - $15.00 USD Received 21 Nov 2011; revised 30 Dec 2011; accepted 30 Dec 2011; published 12 Jan 2012
(C) 2012 OSA

permittivity. As an example, Fig. 1 presents the propagation length of a SP at an Al/sapphire (Al_2O_3) interface (left y-axis) and its effective index (right y-axis). Using realistic values of the dispersion taken from Palik [17], the propagation length and the effective index have been calculated respectively as [18]:

$$L = \left(2\,\mathrm{Im}[k_{SP}(\omega)]\right)^{-1} \text{ and } n_{eff} = \mathrm{Re}[k_{SP}/k_0], \quad (1)$$

where $k_{SP} = k_0\sqrt{\varepsilon_{Al}\varepsilon_{Al2O3}/\left(\varepsilon_{Al}+\varepsilon_{Al2O3}\right)}$ is the Al/Al_2O_3 SP wavevector, ε is the electric permittivity and $k_0 = \omega/c$ is the vacuum wave-vector. The figure indicates that the propagation length drastically decreases in the UV region with a corresponding increase of the magnitude of the SP effective index. In this work we study a simple Al subwavelength grating on an Al_2O_3 substrate (Fig. 2) to estimate UV SERS performance as a function of grating period and laser wavelength. The calculations have been performed using a rigorous electromagnetic approach based on the Fourier-modal method (FMM) [19,20] which lends itself well for calculation of the transmission (*T*), reflection (*R*), absorption (*A = 1-R-T*), and field localization in periodic structures.

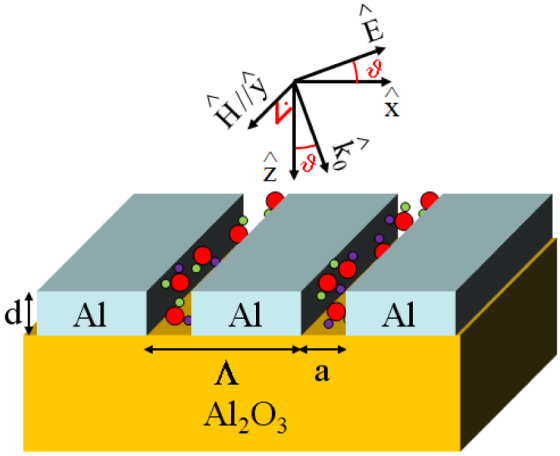

Fig. 2. Geometry: Al metallic grating of thickness d, period Λ and slit aperture a, grown on a sapphire substrate. Inside the slits are positioned generic molecules for SERS. We consider an impinging electromagnetic wave, TM-polarized (H vector parallel to the grooves) with vacuum wavevector k_0 incident at an angle ϑ with respect to the z-axis in the (x,z) plane.

2. Results and discussion

Let us start our analysis by showing in Fig. 3(a-c) the absorption calculated in the plane (ω, k_x) using the FMM for three different structures with periods Λ = 160nm, 128nm, and 96nm. In all three cases, the thickness of the Al grating is d = 50nm, and the slit aperture is a = 16nm. Calculating the absorption of the grating provides useful information about its plasmonic band structure. According to the fluctuation-dissipation theorem [21], the absorption is proportional to the average electric field localization in the metal through the imaginary part of its electric permittivity: $A(\omega) \approx Im(\varepsilon)\langle|E(\omega)|^2\rangle$.

#158512 - $15.00 USD Received 21 Nov 2011; revised 30 Dec 2011; accepted 30 Dec 2011; published 12 Jan 2012
(C) 2012 OSA

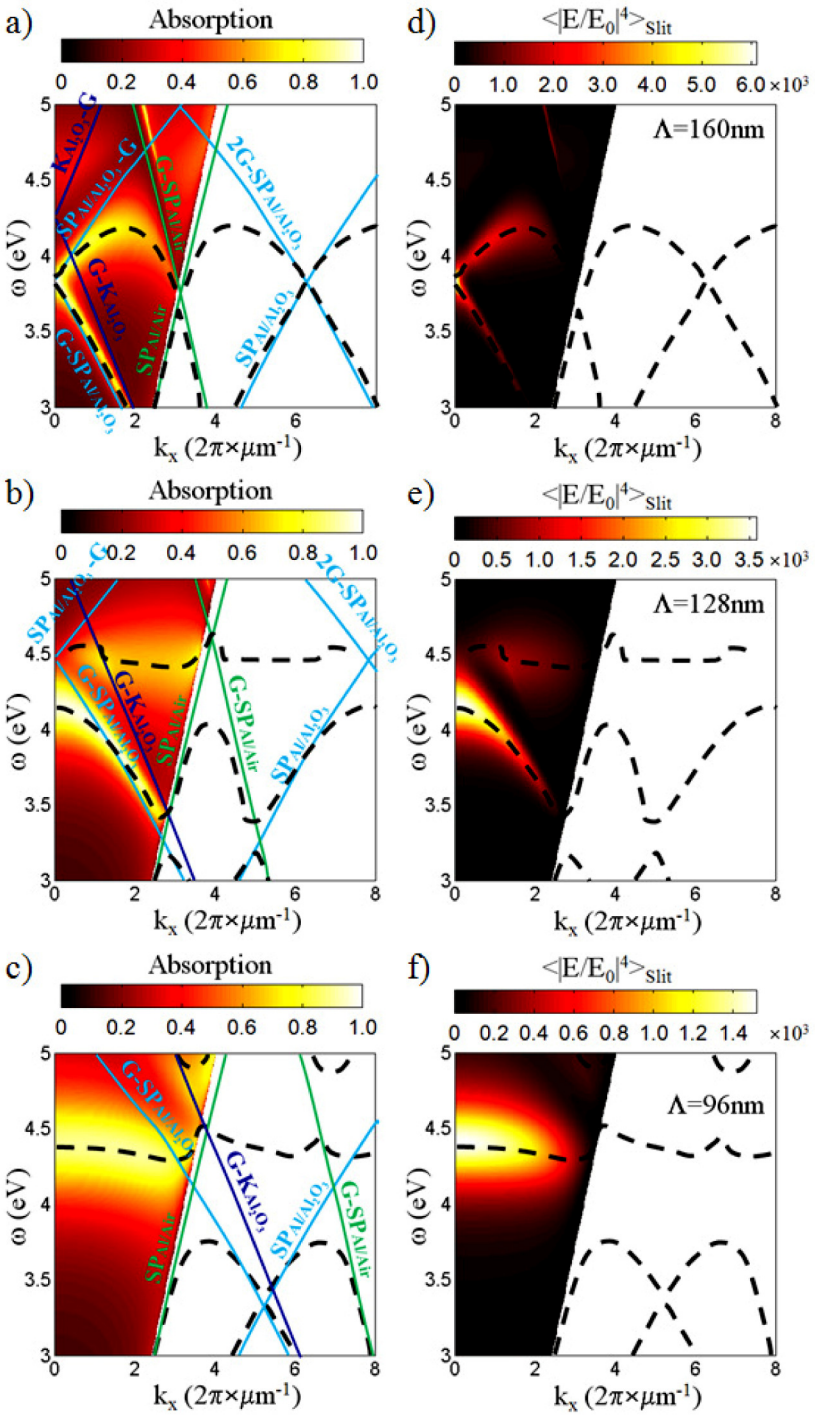

Fig. 3. Left panel: (a-c). Calculated absorption in the (ω,k_x) plane using the FMM for three structures with specified periods. The thickness and slit aperture are the same for all cases: d = 50nm and a = 16nm. Superimposed: (continuous lines) dispersion of the unperturbed air/Al and Al/Al_2O_3 SPs folded along the reciprocal lattice vectors of the grating, and Rayleigh condition for the output medium (K_{Al2O3}-G and G-K_{Al2O3}). The thick-dashed line represents the actual dispersion calculated numerically. Right panel: (d-f). Average Raman enhancement inside the slit for the three structures and the superimposed dispersion (thick-dashed line).

#158512 - $15.00 USD Received 21 Nov 2011; revised 30 Dec 2011; accepted 30 Dec 2011; published 12 Jan 2012
(C) 2012 OSA

Therefore, regions of high absorption are an indication of resonant fields inside the metal. In the figures are also reported the analytical dispersion of the unperturbed Al/Al_2O_3 SP and the unperturbed Al/air SP. Both have been folded in the (ω, k_x) plane using the various reciprocal lattice vectors $G = 2\pi/\Lambda$ of the grating according to $\omega(k_x) = \Omega(|k_{SP} \pm mG|)$. For completeness, the figures also report the dispersion of the Rayleigh condition in the substrate: $\omega(k_x) = \Omega(|k_{Al2O3} \pm mG|)$. In this case the Rayleigh condition corresponds to having the first diffraction order propagate tangentially to the grating at the grating/substrate interface [20]. The actual, full dispersion $\omega = \omega(k_x)$ of the gratings (thick-dashed line) has also been numerically calculated by finding the zeros of the determinant of the respective scattering matrices $|det\ M(\omega, k_x)|$.

Figures 3(a-c) highlight four relevant features. First of all, note that the periodic texturing of the grating modifies the unperturbed dispersion of the Al/Al_2O_3 and air/Al SPs, leading to the formation of plasmonic band gaps in the region of intersection of the unperturbed dispersions. In particular, in the propagation region ($k_x < k_0$), the plasmonic band gap is formed at the intersection of the unperturbed dispersions of the Al/Al_2O_3 SP folded along G and $-G$. The plasmonic band gap is bounded by a low frequency and a high frequency band edge where SP standing waves can be excited [18,22]. This is the classical mechanism that leads to band gap formation, well known in solid-state physics and wave-physics [23].

Second, the numerically calculated dispersion (thick-dashed line) follows the absorption resonances of the structures remarkably well, as expected based on the above-mentioned considerations. In particular, the maximum of the absorption follows the low frequency plasmonic band edge which is located at ω = 3.82eV (λ~325nm) for Λ = 160nm, at ω = 4.16eV (λ~300nm) for Λ = 128nm, and at ω = 4.4eV (λ~280nm) for Λ = 96nm. Third, the spectral position of the plasmonic band edge can be moved toward high frequencies by simply decreasing the period of the grating. Fourth, the spectral width of the plasmonic band gap enlarges as it is pushed toward higher frequencies. It will be seen later that all these characteristics can be described by using a simple, analytical model.

Raman enhancement increases approximately as the fourth power of the modulus of the electric field [5,9,10]. For a molecule randomly positioned inside the slits of the grating the average Raman enhancement is calculated as [24]:

$$Raman\ enhancement = \left\langle \left| E\left(\vec{r}\right) / E_0 \right|^4 \right\rangle_{slit}, \qquad (2)$$

where the symbol $\langle\ \rangle_{slit}$ denotes the spatial average of the field inside the slits and E_0 is the incident electric field. The estimated average Raman enhancements for the three structures are shown in Fig. 3(d-f). The figures show the Raman enhancement in the (ω, k_x) with the dispersion superimposed. The figures make clear that the Raman enhancement follows the plasmonic dispersion of the structure extremely well, with the consistent enhancement in the region near the low frequency plasmonic band edge. Note that the plasmonic dispersion has been calculated from the absorption of the metal structure while the Raman enhancement has been calculated as in Eq. (2), so the two quantities are not in general related to each other. The fact that the Raman enhancement follows the plasmonic dispersion is a clear indication of the dominant role played by the plasmon modes in the cases analyzed.

#158512 - $15.00 USD Received 21 Nov 2011; revised 30 Dec 2011; accepted 30 Dec 2011; published 12 Jan 2012
(C) 2012 OSA

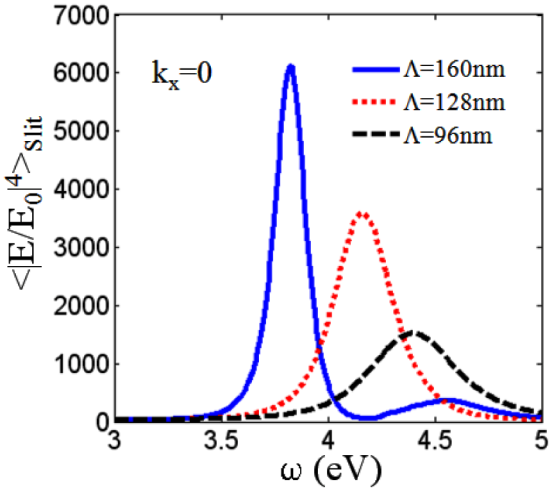

Fig. 4. Average Raman enhancement at normal incidence ($k_x = 0$) for the three structures.

To highlight the resonant characteristics of the process, Fig. 4 summarizes the average Raman enhancement calculated for normal incidence ($k_x = 0$). The enhancement decreases and linewidth broadens as the frequency increases as expected considering the increasing dampening suffered by the Al/Al_2O_3 SP in these cases (see for comparison Fig. 1). For Λ = 160 nm, the propagation length of the SP is still enough to encompass more than ten elementary cells of the grating, while for Λ = 96 nm only few elementary cells are encompassed. Still, even at the highest frequencies, the enhancement factor remains quite large with an average enhancement in the slit of ~10^3.

In Fig. 5 is shown the absolute value of the electric field in an elementary cell of the grating. In particular, Fig. 5 (a-c) plots the normal incidence absolute value of the electric field in logarithmic scale at the frequencies corresponding to the maximum Raman enhancement for the three structures. The field intensity at the Al/Al_2O_3 interface decreases for increasing frequency in agreement with the predicted increase of the damping of the Al/Al_2O_3 SP. For a better perspective, Fig. 5 (d-f) plots instead the same quantity in a 3-D view. Both panels report the position of the "hot spots" where the maximum Raman enhancement is available.

It is shown that these "hot spots" are located near the edges of the grating at the air/Al interface, and their strength gradually decreases for increasing frequency in agreement with the previous results. In general, it is well known that the greatest electromagnetic field localization occurs near imperfections in the form of a metallic tip or step in an otherwise flat surface [10]. In the present cases the "hot spots" are located near the step of the grating at the air/Al interface and, less intensely, at the Al/Al_2O_3 interface. Note that the strength of these "hot spots" is still determined by the strength of the Al/Al_2O_3 SP; in fact, it is found that $|E/E_0|_{Max}$~23 for Λ = 160 nm, $|E/E_0|_{Max}$~19 for Λ = 128 nm, and $|E/E_0|_{Max}$~17 for Λ = 96 nm, corresponding respectively to local Raman enhancements approximately of $23^4 = 2.7\text{x}10^5$, $19^4 = 1.3\text{x}10^5$, and $17^4 = 8\text{x}10^4$. Moreover, the strength of the "hot spots" depends on the thickness of the Al grating d. As d increases, Ohmic losses increase and the electromagnetic field funneled inside the slits is increasingly dissipated. Conversely, as d decreases the electromagnetic field is less effectively funneled through the slits, while a portion of the field continues to be dissipated by Ohmic losses in the metal itself. The result is the same in both cases: a decreased coupling efficiency of the field to the Al/Al2O3 SP and a reduced intensity of the "hot spots." The optimal thickness for the formation of the "hot spots" comes from a balance of these two effects and must be assessed on a case by case basis.

#158512 - $15.00 USD Received 21 Nov 2011; revised 30 Dec 2011; accepted 30 Dec 2011; published 12 Jan 2012
(C) 2012 OSA

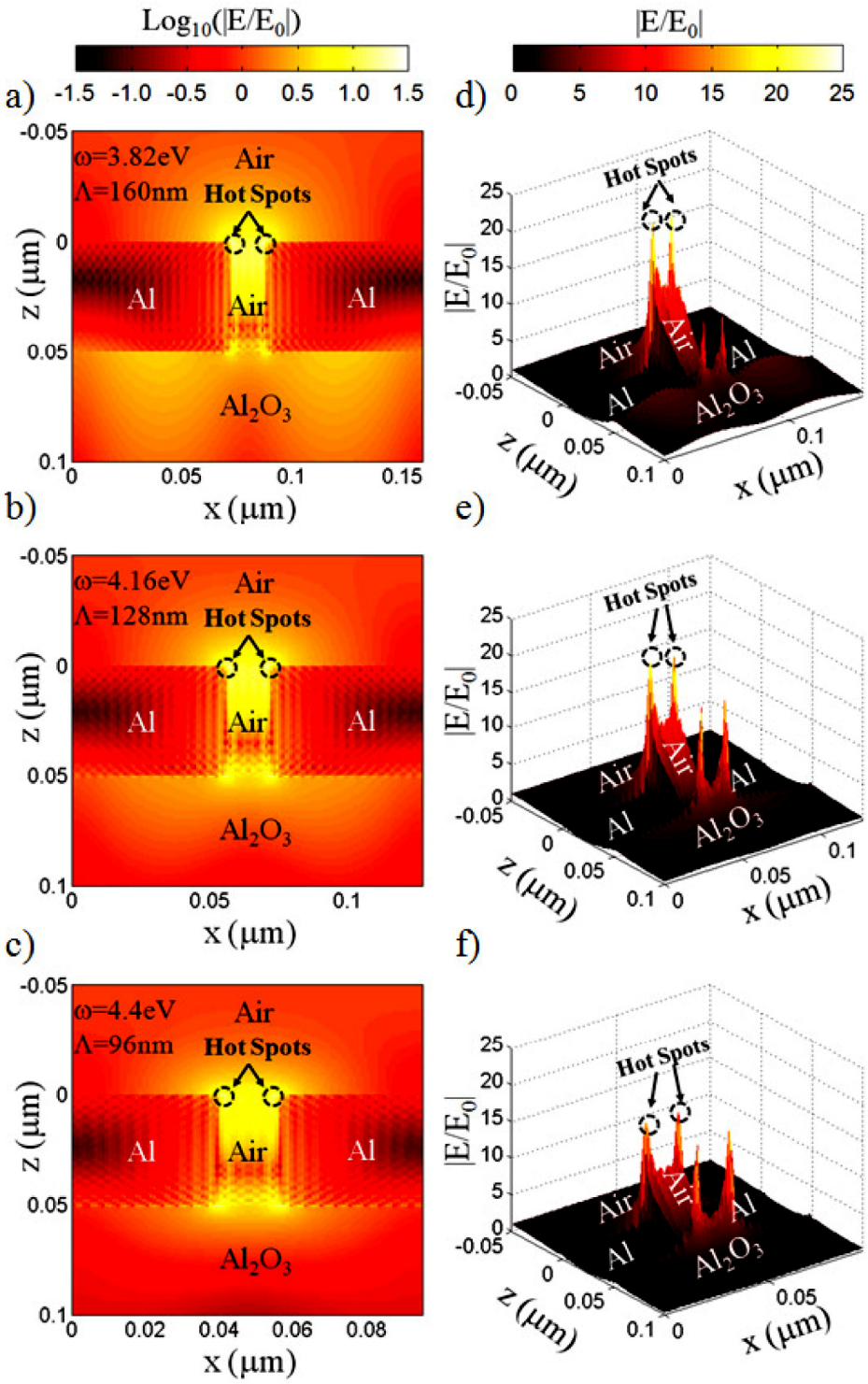

Fig. 5. Left panel: (a-c). 2-D view of the absolute value of the electric field in logarithmic scale at the frequencies corresponding respectively to the maximum Raman enhancement for the three structures. Right panel (d-f). 3-D view of the absolute value of the electric field in linear scale. In both panels the position of the "hot spots" is indicated.

#158512 - $15.00 USD Received 21 Nov 2011; revised 30 Dec 2011; accepted 30 Dec 2011; published 12 Jan 2012
(C) 2012 OSA

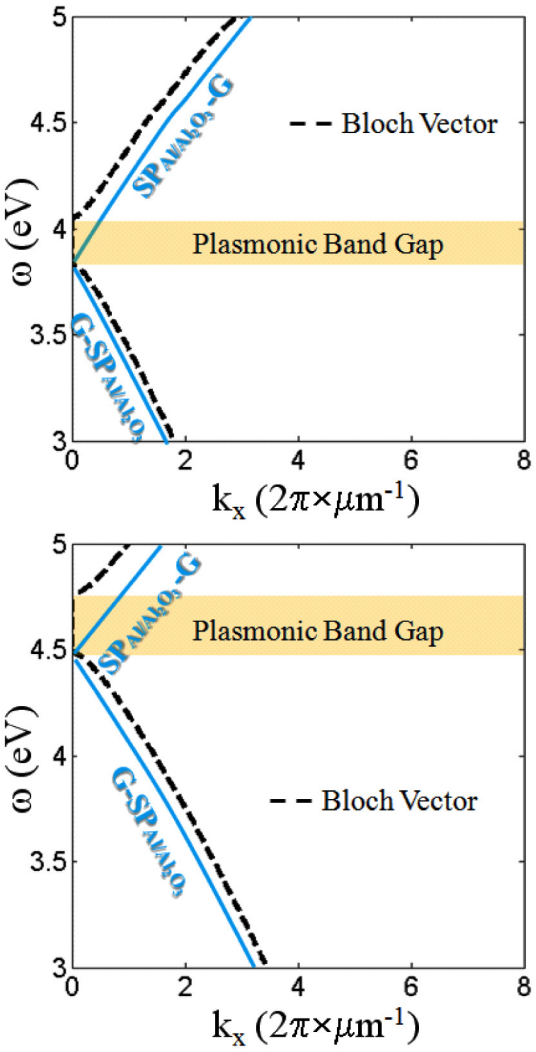

Fig. 6. Dispersion (dashed line) for the structure with Λ = 160nm (upper figure) and with Λ = 128nm (lower figure) calculated through the Bloch vector as in Eq. (3). For comparison, the figures also report the unperturbed dispersion (solid line) of the Al/Al_2O_3 SP coupled respectively with *G* and *–G*.

The position of the plasmonic band edge and the width of the band gap can be recaptured by the following simple analytical dispersion model that uses the Bloch vector K_β of an ideal 1-D, multilayered structure [25]:

$$\cos(K_\beta \Lambda) = \cos(k_a a)\cos(k_b b) - \frac{1}{2}\left(\frac{n_b}{n_a} + \frac{n_a}{n_b}\right)\sin(k_a a)\sin(k_b b), \qquad (3)$$

where b = Λ-a, $k_a = k_0$, $k_b = n_{eff}\, k_0$, $n_a = 1$, and $n_b = n_{eff}$ which is the effective index of the Al/Al_2O_3 SP as calculated in Fig. 1. Figure 6 shows the plasmonic band gap position predicted by the Bloch vector approach as in Eq. (3) for the structures with periods Λ = 160 nm and 128 nm, respectively. Comparing Fig. 6 with the plots in Fig. 3 for the first two structures, note how the position and width of the plasmonic band gap are predicted with remarkable accuracy, especially considering that the analytical model does not take into account the finite thickness of the Al grating and neglects the damping of the SP. This simple model confirms

#158512 - $15.00 USD Received 21 Nov 2011; revised 30 Dec 2011; accepted 30 Dec 2011; published 12 Jan 2012
(C) 2012 OSA

the notion of a plasmonic band edge and provides a simple tool for estimating the grating pitch that will produce the greatest Raman enhancements for a given UV laser frequency. In particular, the enlargement of the plasmonic band gap for higher frequencies can be ascribed to the increasing index contrast between the "air layers" and n_{eff} of the "plasmonic layers" (see Fig. 1), in complete analogy with the band gap of conventional 1-D multilayered structures [25].

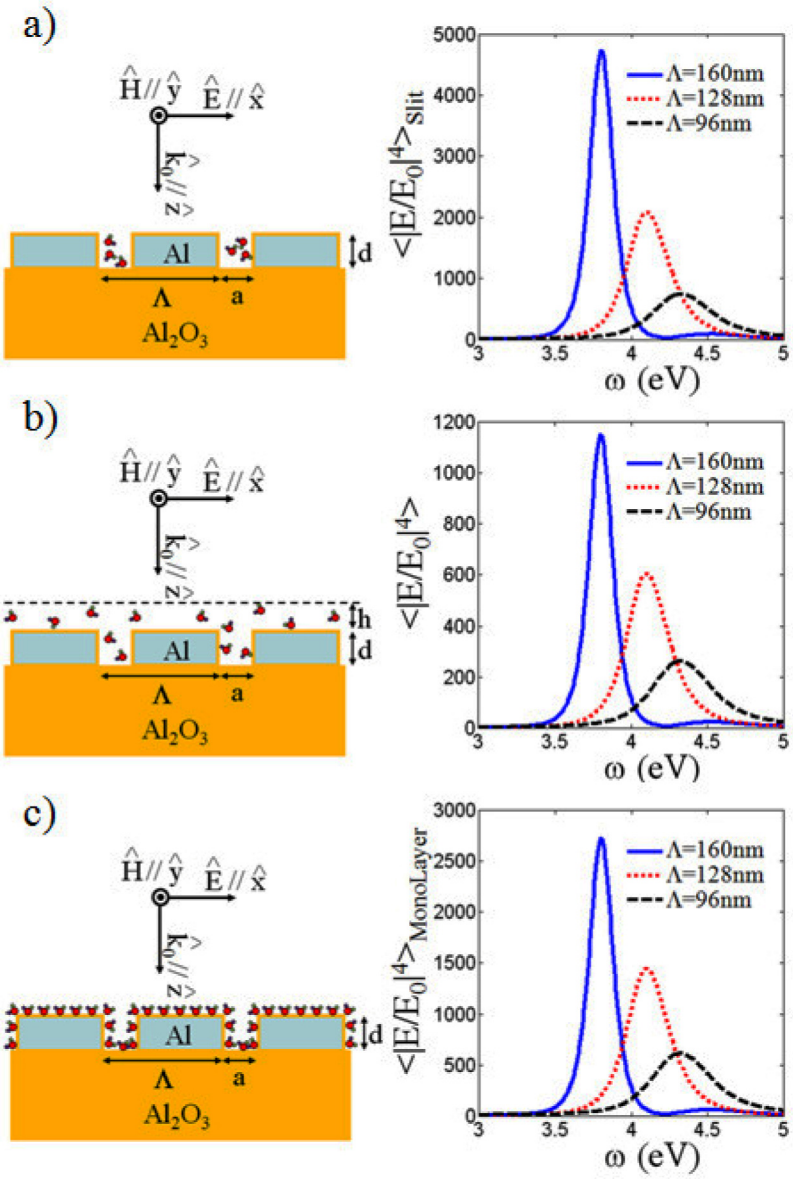

Fig. 7. Average Raman enhancement at normal incidence ($k_x = 0$) for the three structures in the case of a) Al grating with a 2nm Al_2O_3 overlayer and molecules positioned inside the slits; b) Al grating with Al_2O_3 overlayer and molecules positioned inside the slits and in a region above the grating with h = 20nm; c) Al grating with Al_2O_3 overlayer and self-assembled monolayer 3nm thick.

The kind of structures proposed in this work can be fabricated using current nanofabrication techniques. Aluminum gratings will rapidly oxidize upon exposure to air and

#158512 - $15.00 USD Received 21 Nov 2011; revised 30 Dec 2011; accepted 30 Dec 2011; published 12 Jan 2012
(C) 2012 OSA

will typically be coated by a 2-3nm layer of Al_2O_3 [13,26,27]. Figure 7(a) reports the average Raman enhancement for molecules inside the slits with the oxide overlayer, and the results should be compared with those reported in Fig. 4 for the bare grating. Notice that the reduction in the Raman enhancement caused by the oxide overlayer becomes more severe as Λ decreases. The effect of the oxide on the average Raman enhancement has also been calculated for two experimentally relevant cases: the molecules occupy a region that includes the slits and some space above the grating (Fig. 7(b)), and the molecules form a self-assembled monolayer 3nm thick (Fig. 7(c)). The figures show how the salient physical characteristics of the Raman enhancement are basically preserved under the various circumstances mentioned above, although the degree of enhancement depends on the spatial separation between the plasmon and the analyte [28]. This is another indication of the dominant role played by the plasmonic band edge associated to each structure.

3. Conclusions

In conclusion, we have studied UV SERS for an Al grating grown on a sapphire substrate and shown that, despite large ohmic losses, large Raman enhancement factors can be achieved by operating at the plasmonic band edge. An analytic dispersion model accurately reproduces the calculated plasmonic band edge and provides a simple tool for estimating the grating pitch to produce optimal Raman enhancement for a given UV laser. Note that the methodology presented here has a general validity and therefore we should expect similar results for properly designed gratings made of other metals like Ga and In [29], for example, opening new venues for UV SERS.

Acknowledgments.

N.M., G.D. and M.C.B. acknowledge financial support from DARPA SBIR project "Nonlinear Plasmonic Devices" contract number W31P4Q-11-C-0109.

#158512 - $15.00 USD Received 21 Nov 2011; revised 30 Dec 2011; accepted 30 Dec 2011; published 12 Jan 2012
(C) 2012 OSA